European Archives of Oto-Rhino-Laryngology (2018) 275:2151–2157
https://doi.org/10.1007/s00405-018-5052-y

HEAD & NECK

Histogram analysis of apparent diffusion coefficient maps for differentiating malignant from benign parotid gland tumors

Gao Ma[1] · Liu-Ning Zhu[2] · Guo-Yi Su[1] · Hao Hu[1] · Wen Qian[1] · Shou-Shan Bu[2] · Xiao-Quan Xu[1] · Fei-Yun Wu[1]

Received: 10 April 2018 / Accepted: 28 June 2018 / Published online: 2 July 2018

Abstract

Purpose To evaluate the diagnostic performance of histogram parameters derived from diffusion-weighted imaging (DWI) for differentiating malignant from benign parotid gland tumors compared with that of hotspot region of interest (ROI)-based apparent diffusion coefficient (ADC) measurement.

Methods Our study retrospectively enrolled 60 patients with parotid gland tumors who had undergone DWI scan for pre-treatment evaluation. ADC measurements were performed using hotspot ROI ($ADC_{HS\text{-}ROI}$)-based and histogram-based approach. Histogram parameters included mean (ADC_{mean}), median (ADC_{median}), 10th (ADC_{10}), 90th (ADC_{90}) percentiles, skewness and kurtosis of ADC. Mann–Whitney *U* test, Kruskal–Wallis test with post hoc Dunn–Bonferroni method and receiver operating characteristic (ROC) curve analyses were used for statistical analyses.

Results $ADC_{HS\text{-}ROI}$ and ADC histogram parameters showed no significant differences between malignant and benign parotid gland tumors (All $Ps > 0.05$). Within the sub-group analyses, Warthin's tumors showed the lowest $ADC_{HS\text{-}ROI}$, ADC_{mean}, ADC_{median}, ADC_{10} and ADC_{90} value, followed by malignant tumors and pleomorphic adenomas (All $Ps < 0.05$). ADC_{10} out-performed $ADC_{HS\text{-}ROI}$ in differentiating malignant tumors from pleomorphic adenomas (area under curve, 0.890 vs 0.821; sensitivity, 79.31 vs 82.76%; specificity, 90.91 vs 72.73%; $P = 0.016$), and improved the diagnostic performance in differentiating malignant tumors from Warthin's tumors (area under curve, 1.000 vs 0.965; sensitivity, 100.00 vs 90.91%), although the difference was not significant ($P = 0.348$).

Conclusions ADC histogram analysis, especially ADC_{10}, might be a promising imaging biomarker for characterizing parotid gland tumors.

Keywords Parotid gland tumor · Magnetic resonance imaging · Diffusion-weighted imaging · Histogram

Introduction

Parotid gland tumors contain a heterogeneous group of benign and malignant subtypes [1]. Accurate differentiation between malignancy and benignity is important for the determination of therapeutic strategy and prediction of disease prognosis [2]. Due to the higher risk of malignant degeneration and of recurrence, the differentiation between pleomorphic adenomas and Warthin's tumors also influence the determination of surgical approach [3, 4]. Ultrasound plays important roles in the initial assessment of parotid tumors and guiding fine needle aspiration cytology. However, ultrasound is limited to superficial structures and accuracy depends on specialist expertise [5]. Computed tomography (CT) and magnetic resonance imaging (MRI) are optimal to evaluate the complete tumor extent and commonly used for diagnostic purpose. Several

Gao Ma and Liu-Ning Zhu contributed equally to this work.

✉ Xiao-Quan Xu
xiaoquanxu_1987@163.com

✉ Fei-Yun Wu
wfy_njmu@163.com

[1] Department of Radiology, The First Affiliated Hospital of Nanjing Medical University, No. 300, Guangzhou Rd., Gulou District, Nanjing, People's Republic of China

[2] Department of Stomatology, The First Affiliated Hospital of Nanjing Medical University, Nanjing, People's Republic of China

imaging features such as ill-defined, infiltrative border, heterogeneous internal signal with cystic change and necrosis have been reported to be helpful in predicting aggressive parotid gland tumors [3–5]. However, the differentiating value of these imaging features from conventional structural CT and MRI is still on debate due to the unsatisfactory reproducibility [6].

Recently, various functional MR imaging techniques have been proven to be useful for quantifying tumor characteristics related to tumor physiology and biology [7]. Among these, diffusion-weighted imaging (DWI) and the derived apparent diffusion coefficient (ADC) value have been commonly used to characterize parotid gland tumors [8–11]. DWI and its derived ADC value can provide quantitative information about Brownian motion in tissues. Generally, increased cellularity and decreased interstitial space in tissue will lead to a limited Brownian motion, and subsequently a lower ADC value [8].Yuan et al. reported that the mean values of malignant parotid gland tumors were significantly lower than those of benign tumors [11]. However, Habermann et al. indicated that there was a significant overlap of mean ADCs within the group of benign and malignant parotid gland tumors [4]. Thus, the efficacy of DWI and ADC in the differential diagnosis of parotid gland tumors has not been fully established.

In previous studies, mean ADCs was usually used for differentiation. The most notable advantage of using mean ADC as imaging biomarker is its convenience and speediness; however, it ignored the tumor heterogeneity [12].

As a novel technique to analyze the parametric maps, histogram analysis based on pixel distribution can supply added information about the tumor heterogeneity. It has been proved to be a superior tool for tumor diagnosis, grade, stage and prognosis prediction in various organs [13–16]. However, to the best of our knowledge, the application of DWI with histogram analysis for differentiating malignant from benign parotid gland tumors has not been reported till now.

Therefore, the purpose of this study was to evaluate the diagnostic performance of histogram analysis of ADC maps for differentiating between malignant and benign parotid gland tumors.

Materials and methods

Study population

This study was approved by Institutional Review Board of our hospital. Requirement of written informed consent was waived due to the retrospective nature of our study. From January 2017 to December 2017, 73 patients underwent MR imaging examination for pre-surgery evaluation of parotid gland tumors. According to the following exclusion criteria: (1) lack of DWI ($n=3$); (2) biopsy was administered before MR scan ($n=1$); (3) pure cystic lesion ($n=5$); (4) short-axis diameter of the tumor was less than 1 cm ($n=2$); and (5) presence of severe motion artifacts ($n=2$), 13 patients were excluded. Finally, a total of 60 patients (31 men, 29 women; age range 10–85 years; mean age 50.6 ± 17.4 years) were enrolled in this study. Among these, 49 patients had benign parotid gland tumors and 11 had malignant tumors. All these tumors were diagnosed via pathological examinations after surgery. The demographic and pathological characteristics of all patients are summarized in Table 1.

MRI protocol

MRI examinations were performed with a 3.0 T MR scanner (MAGNETOM skyra, Siemens Healthcare, Erlangen, Germany) with a 12-channel head and neck coil. The images included: (1) axial T2-weighted image [repetition time (TR)/echo time (TE), 4000/85 ms; slice number, 25; slice thickness, 4 mm without gap; field of view (FOV), 200 mm; matrix, 384×384]; (2) axial T1-weighted image (TR/TE,

Table 1 Summary and comparison of the demographic and pathological characteristics of parotid gland tumors

Characteristics	Benign group ($n=49$)	Malignant group ($n=11$)	P value
Demographics			
Male/female	24/25	7/4	0.294
Age (years)	50.9 ± 17.0	49.3 ± 19.8	0.500
Lesion size (cm)	2.267 ± 0.962 (range 1.020–4.520)	2.450 ± 1.227 (range 1.130–4.320)	0.717
Pathology	Pleomorphic adenoma (29)	Mucoepidermoid carcinoma (2)	
	Warthin's tumor (13)	Acinic cell carcinoma (4)	
	Base cell adenoma (4)	Ductal carcinoma (1)	
	Oncocytic adenoma (1)	Metastatic melanoma (1)	
	Myofibroblastoma (1)	Malignant myoepithelioma (1)	
	Cavernous hemangioma (1)	Metastatic squamous carcinoma (2)	

Data are reported as mean ± standard deviation; data in parentheses indicate the number of corresponding patients in our study

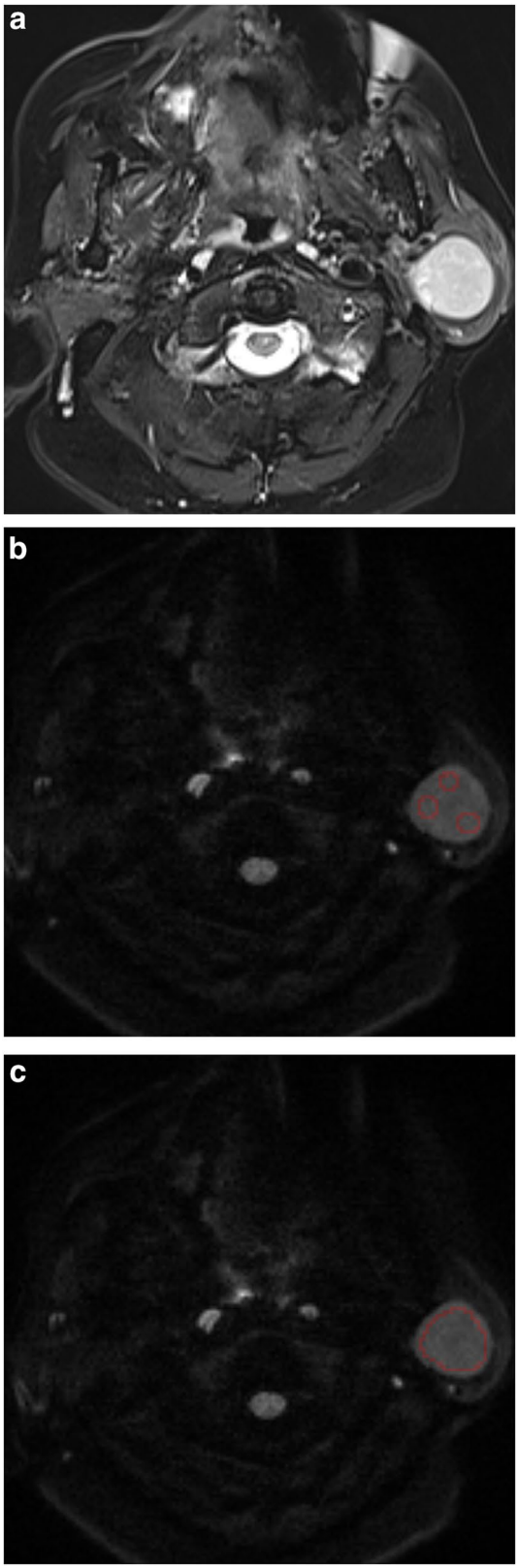

Fig. 1 Schematic diagram of the placements of ROIs. **a** Axial T2-weighted image with fat suppression of base cell adenoma in the left parotid gland. **b** In terms of hotspot ROI- based mean ADC measurements, the slice on which the tumor showed the biggest diameter was chosen. Three free-hand circular ROIs were placed on the tumor area which demonstrates mostly increased signal intensity on DW image (b_{1000} map). **c** In terms of ADC histogram analysis, irregular ROIs were manually placed on all DW imaging (b_{1000} map) slices to encompass the whole tumor. The selection method in a typical slice was exhibited

800/6.7 ms; slice number, 25; slice thickness, 4 mm without gap; FOV, 200 mm; matrix, 384 × 384); and (3) coronal fat-suppressed T2-weighted image (TR/TE, 4000/75 ms; slice number, 20; slice thickness, 4 mm without gap;y FOV, 200 mm; matrix, 384 × 384).

Readout-segmented echo planar imaging sequence was used for DWI scan with two *b* values (0 and 1000 s/mm^2) in three orthogonal directions. The imaging parameters were as follows: diffusion schema, Stejskal–Tanner; fat suppression, frequency selective; TR/TE, 3000/69 ms; slice number, 20; number of excitations, 1; FOV, 200 mm; slice thickness, 4 mm without gap; matrix, 224 × 224; phase-encoding direction, anteroposterior; echo spacing, 0.4 ms; number of readout segments, 5; total acquisition time, 2 min 20 s.

Imaging analysis

Diffusion-weighted imaging data were processed using an in-house developed software (FireVoxel, CAI^{2}R, New York University, NY, USA) with mono-exponential model.

The largest diameter of the lesions was measured on axial T2-weighted image. In terms of hotspot regions of interest (ROIs)-based mean ADC measurements ($ADC_{HS\text{-}ROI}$), the slice on which the tumor showed the biggest diameter was chosen. Three free-hand circular ROIs were placed on the tumor area which demonstrates mostly increased signal intensity on DW image (b_{1000} map). In terms of ADC histogram analysis, irregular ROIs were manually placed on all DW imaging (b_{1000} map) slices to encompass the whole tumor. Histogram analysis of ADC was performed using PASW Statistics 18.0 (SPSS, Chicago, IL, USA). Following histogram parameters were derived: (1) mean; (2) median; (3) kurtosis, the degree of the peakedness of the histogram distribution; (4) skewness, a measure of the degree of asymmetry of the histogram distribution. The parameters of 10th and 90th percentiles of ADC were derived for the cumulative histogram. The *n*th percentile was the point at which *n*% of the voxel values that form the histogram were found to the left. A representative case for introducing two ROIs selection methods during hotspot ROI-based and histogram-based ADC measurements is shown in Fig. 1.

During ROIs placement, obvious cystic, necrotic and hemorrhagic component of the tumor was excluded with reference to T2-weighted images. To reduce the influence of partial volume effect, the ROIs were slightly smaller in size than the actual mass size. If multiple lesions occurred, the

lesion with the largest diameter was chosen for analysis. All the ROIs were individually delineated by two radiologists (reader 1: with 7 years; reader 2: with 3 years of clinical experience in head and neck radiology) who were blind to the pathological diagnosis and study design. The average of the two measurement results was used for further statistical analysis.

Statistical analysis

All numeric data were reported as mean ± standard deviation. The normality of the quantitative parameters was tested with Kolmogorov–Smirnov's test. Chi-square test was used to compare the difference of gender between malignant and benign groups. Mann–Whitney *U* test was used to compare the differences of age, tumor size and ADC values between two groups. Kruskal–Wallis test with post hoc Dunn–Bonferroni method was used for the comparisons of ADC values among pleomorphic adenomas, Warthin's tumors and malignant tumors. Receiver operating characteristic (ROC) curve analyses were performed to evaluate the diagnostic value of significant parameters. Areas under the ROC curves (AUCs) were compared using published method [17]. Statistical analysis was carried out using statistical packages (SPSS Version 23.0, SPSS, Chicago, IL, USA; and MedCalc version 11.0, MedClac, Mariakerke, Belgium). A two-sided *P* value less than 0.05 was set as statistical significance.

Results

There was no significant difference in age distribution ($P=0.500$), gender distribution ($P=0.294$) and tumor size ($P=0.717$) between malignant and benign groups.

Malignant tumors vs benign tumors

Detailed $ADC_{HS\text{-}ROI}$ and ADC histogram parameters obtained between malignant and benign parotid gland tumors are summarized in Table 2. No significant difference was found in $ADC_{HS\text{-}ROI}$, ADC_{mean}, ADC_{median}, ADC_{10}, ADC_{90}, skewness and kurtosis between malignant and benign groups (All Ps > 0.05).

Malignant tumors vs pleomorphic adenomas

Malignant tumors showed significantly lower $ADC_{HS\text{-}ROI}$, ADC_{mean}, ADC_{median} and ADC_{10} than pleomorphic adenomas, while there was no significant difference in ADC_{90}, skewness and kurtosis between two groups (Table 2).

Detailed diagnostic performance of $ADC_{HS\text{-}ROI}$ and significant ADC histogram parameters are summarized in Table 3. ADC_{10} (AUC, 0.890; cut-off value, 0.959×10^{-3} mm^2/s; sensitivity, 79.31%; specificity, 90.91%) demonstrated significantly better diagnostic performance than $ADC_{HS\text{-}ROI}$ ($P=0.016$), ADC_{mean} ($P=0.016$) and ADC_{median} ($P=0.016$) for differentiating between malignant tumors and pleomorphic adenomas.

Malignant tumors vs Warthin's tumors

Malignant tumors showed significantly higher $ADC_{HS\text{-}ROI}$, ADC_{mean}, ADC_{median}, ADC_{10} and ADC_{90} than that of Warthin's tumors, while there was no significant difference in skewness and kurtosis between two groups (Table 2).

ADC_{10} showed the optimal performance for differentiating malignant tumors from Warthin's tumors (cut-off value, 0.630×10^{-3} mm^2/s; AUC, 1.000; sensitivity, 100.00%; specificity, 100.00%), although the difference in AUC between

Table 2 Multiple comparison among pleomorphic adenomas, Warthin's tumors and malignant tumors

Parameters	Benign tumors	Malignant tumors	Pleomorphic adenomas	Warthin's tumors	*P* value			
					Malignant tumors vs benign tumors	Malignant tumors vs pleomorphic adenomas	Malignant tumors vs Warthin's tumors	Pleomorphic adenomas vs Warthin's tumors
$ADC_{HS\text{-}ROI}$	1.177 ± 0.421	1.035 ± 0.145	1.391 ± 0.074	0.741 ± 0.019	0.374	0.045	0.029	< 0.001
ADC histogram								
ADC_{mean}	1.217 ± 0.423	1.078 ± 0.173	1.442 ± 0.070	0.756 ± 0.026	0.364	0.032	0.042	< 0.001
ADC_{median}	1.208 ± 0.433	1.068 ± 0.168	1.432 ± 0.075	0.752 ± 0.024	0.406	0.046	0.031	< 0.001
ADC_{10}	1.018 ± 0.440	0.868 ± 0.108	1.252 ± 0.070	0.513 ± 0.036	0.160	0.013	0.049	< 0.001
ADC_{90}	1.428 ± 0.454	1.303 ± 0.165	1.682 ± 0.073	0.922 ± 0.027	0.560	0.056	0.023	< 0.001
Skewness	0.138 ± 0.603	0.419 ± 0.728	0.061 ± 0.701	0.192 ± 0.432	0.256	0.232	0.284	0.713
Kurtosis	0.531 ± 1.186	0.779 ± 0.706	0.632 ± 1.345	0.574 ± 1.074	0.057	0.119	0.213	0.724

Data are reported as mean ± standard deviation; the unit for ADC value is $\times10^{-3}$ mm^2/s

ADC apparent diffusion coefficient, ADC_n *n*th percentile value of accumulative ADC histogram

Table 3 Diagnostic performance of ADC histogram parameters in discriminating parotid gland tumors

Parameters	Cut-off value	Area under curve	Sensitivity (%)	Specificity (%)
Discriminating malignant tumors from pleomorphic adenomas				
ADC_{HS-ROI}	≤1.077	0.821	82.76	72.73
ADC histogram				
ADC_{mean}	≤1.077	0.821	82.76	72.73
ADC_{median}	≤1.077	0.821	82.76	72.73
ADC_{10}	≤0.959	0.890	79.31	90.91
Discriminating malignant tumors from Warthin's tumors				
ADC_{HS-ROI}	>0.860	0.965	90.91	100.00
ADC histogram				
ADC_{mean}	>0.860	0.965	90.91	100.00
ADC_{median}	>0.860	0.965	90.91	100.00
ADC_{10}	>0.630	1.000	100.00	100.00
ADC_{90}	>1.020	0.979	100.00	84.62
Discriminating pleomorphic adenomas from Warthin's tumors				
ADC_{HS-ROI}	>0.860	1.000	100.00	100.00
ADC histogram				
ADC_{mean}	>0.860	1.000	100.00	100.00
ADC_{median}	>0.860	1.000	100.00	100.00
ADC_{10}	>0.630	1.000	100.00	100.00
ADC_{90}	>1.130	0.999	96.55	100.00

The unit for ADC value is $\times 10^{-3}$ mm^2/s

ADC apparent diffusion coefficient, ADC_n *n*th percentile value of cumulative ADC histogram

ADC_{10} and ADC_{HS-ROI} ($P=0.348$) did not reach statistical significance (Table 3).

Pleomorphic adenomas vs Warthin's tumors

Pleomorphic adenomas showed significantly higher ADC_{HS-ROI}, ADC_{mean}, ADC_{median}, ADC_{10} and ADC_{90} than Warthin's tumors, while no significant difference was found in skewness and kurtosis between two groups (Table 2).

ROC analyses results showed that set $ADC_{10} > 0.630 \times 10^{-3}$ mm^2/s as cut-off value, both sensitivity and specificity are 100.00% in discrimination between pleomorphic adenomas and Warthin's tumors, although the difference in differentiating performance between ADC_{10} and ADC_{HS-ROI} ($P=1.000$) did not reach statistical significance (Table 3). Representative cases of acinic cell carcinoma, pleomorphic adenoma and Warthin's tumor are presented in Fig. 2.

Discussion

Our study found that ADC_{HS-ROI} and ADC histogram parameters showed no significant differences between malignant and benign parotid gland tumors. However, within sub-group analyses, Warthin's tumors showed lowest ADC values, followed by malignant tumors and pleomorphic adenomas. ADC_{10} out-performed ADC_{HS-ROI} in differentiating malignant tumors from pleomorphic adenomas or Warthin's tumors. ADC_{10} might be a promising imaging biomarker for characterizing parotid gland tumors.

In agreement with previous studies [2, 18], ADC_{HS-ROI} and ADC histogram parameters showed no significant differences between malignant and benign parotid gland tumors. The most common tumors within benign group were Warthin's tumor and pleomorphic adenomas. Compared with malignant tumors, Warthin's tumor usually showed lower while pleomorphic adenomas usually demonstrated higher ADC value [2]. The diffusion values of benign group represented the mixed mean values of pleomorphic adenomas and Warthin's tumors, therefore, it was not surprising that there was no significant difference in ADC values between malignancy and benignity. These results indicated that ADC values might not be a robust imaging parameter for the differentiation between malignant and benign parotid tumors.

Consistent with previous studies [9, 19], our study also found that Warthin's tumors showed lowest ADC value, followed by malignant tumors and pleomorphic adenomas. Lower ADC values of Warthin's tumors might be relative to the hypercellular matrix caused by epithelial proliferation with lymphocytic infiltration [20]. While higher ADC values of pleomorphic adenomas might be associated with relative abundance of myxoid and chondroid matrices [2, 4]. Within

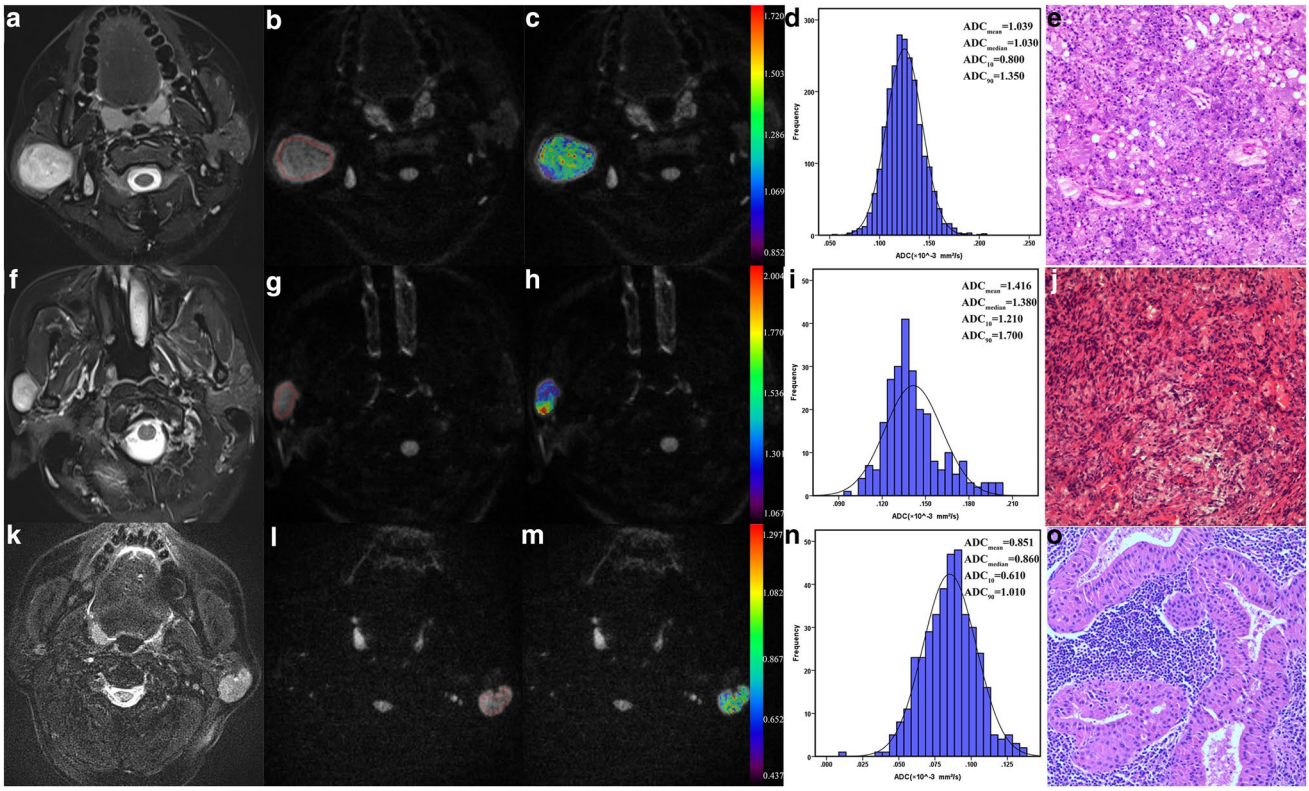

Fig. 2 Representative images of a 58-year-old man with acinic cell carcinoma (**a–e**), a 39-year-old woman with pleomorphic adenoma (**f–j**) and a 71-year-old man with Warthin's tumor (**k–o**). The left column was the axial T2-weighted image with fat suppression (**a, f, k**). After the ROIs were placed (**b, g, l**), colored ADC maps were conducted and embedded into the diffusion images (b_{1000} map) (**c, h, m**). Corresponding histogram maps showed a relatively lower ADC value of Warthin's tumor (**n**), followed by acinic cell carcinoma (**d**), and pleomorphic adenoma (**i**). All the diagnoses were confirmed by histological examination (**e, j, o**)

the sub-group analysis, the difference of ADC_{90} between pleomorphic adenomas and malignant tumors did not reach statistical significance. In our opinion, it might be due to the heterogeneous nature of the malignancy [12]. When we placed the ROIs, obvious cystic, necrotic and hemorrhagic areas were excluded. However, this exclusion process was performed based on the conventional MR images, not the pathological examination. Therefore, some micro-hemorrhagic or micro-necrotic components which were more commonly seen in malignant tumors, would be included for further imaging analysis. This might lead to substantially increased ADC_{90} of malignant parotid tumors, and then resulted in no significant difference of ADC_{90} between pleomorphic adenomas and malignant tumors.

Due to its simplicity, hotspot ROIs were commonly used for ADC measurements in clinical practice and previous studies [9, 21]. However, the major limitation of this approach was its lower reproducibility, which can be overcome by whole-tumor ROI method [22]. In our study, ADC_{10} out-performed $ADC_{HS\text{-}ROI}$ in differentiating malignant tumors from pleomorphic adenomas or Warthin's tumors. The superior performance of low percentile of diffusion parameters had been reported in previous studies [12, 13]. Xu et al. reported that ADC_{10} showed better performance than ADC_{mean} for differentiating malignant from benign orbital tumors [12]. Similarly, Suo et al. indicated that ADC_{min} and ADC_{25} out-performed ADC_{mean} or ADC_{median} for differentiating malignant from benign breast masses [13]. We assumed that the low-percentile ADC values represented better with the focal tumor area with high cell density, which usually represented the most aggressive component within the mass. Therefore, ADC_{10} would naturally demonstrate better differentiating performance.

Some limitations should be noted in our study. First, it was a retrospective study with a relatively small sample size. Second, given the wide variety of histological types and small number of each type, some crucial sub-group differentiation among malignant or benign parotid gland tumors could not to be performed. Further studies with large cohort were needed to clarity the value of DWI in such sub-group differentiation work. Third, despite using the whole-volume ROI and covering as much as tumor area, the placement of ROIs was still performed in a manual pattern. Manual imaging process could result in a potential sampling bias, and

also a long processing time. Future studies using computer-aided imaging analysis might be more valuable. Forth, the placement of ROIs was performed based on the conventional MR images, not the pathological examination, which would influence on the statistical power and the application of the derived threshold value of ADC histogram parameters. Fifth, the threshold value obtained in this study would not be valid for other studies in different institutions with different equipment or *b* values; we believe that multicenter study with large cohort in the future will hopefully confirm our results.

In conclusion, our study showed that ADC histogram parameters could help to differentiate among malignant tumors, pleomorphic adenomas and Warthin's tumors. ADC_{10} might be a promising imaging biomarker for characterizing parotid gland tumors.

Funding This work was supported by National Natural Science Foundation of China (81771796 to FY Wu), and Jiangsu Province's Young Medical Talents Program (QNRC2016560 to Xu XQ).

Compliance with ethical standards

Conflict of interest The authors declare that they have no conflict of interest.

References

1. El-Naggar AK (2017) WHO classification of tumors of salivary glands. In: El-Naggar AK, Chan JKC, Grandis JR, Takata T, Slootweg PJ (eds) WHO classification of head and neck tumours, 4th edn. IARC, Lyon, p 160
2. Takumi K, Fukukura Y, Hakamada H et al (2017) Value of diffusion tensor imaging in differentiating malignant from benign parotid gland tumors. Eur J Radiol 95:249–256
3. Yabuuchi H, Matsuo Y, Kamitani T et al (2008) Parotid gland tumors: can addition of diffusion-weighted MR imaging to dynamic contrast-enhanced MR imaging improve diagnostic accuracy in characterization? Radiology 249:909–916
4. Habermann CR, Arndt C, Graessner J et al (2009) Diffusion-weighted echo-planar MR imaging of primary parotid gland tumors: is a prediction of different histologic subtypes possible? AJNR Am J Neuroradiol 30:591–596
5. Lee YYP, Wong KT, King AD, Ahuja AT (2008) Imaging of salivary gland tumours. Eur J Radiol 66:419–436
6. Eida S, Sumi M, Nakamura T (2010) Multiparametric magnetic resonance imaging for the differentiation between benign and malignant salivary gland tumors. J Magn Reson Imaging 31:673–679
7. Jansen JF, Parra C, Lu YG, Shukla-Dave A (2016) Evaluation of head and neck tumors with functional MR imaging. Magn Reson Imaging Clin N Am 24:123–133
8. Kikuchi M, Koyasu S, Shinohara S, Imai Y, Hino M, Naito Y (2016) Preoperative diagnostic strategy for parotid gland tumors using diffusion-weighted MRI and technetium-99m pertechnetate scintigraphy: a prospective study. PLoS One 11:e0148973
9. Eida S, Sumi M, Sakihama N, Takahashi H, Nakamuraet T (2007) Apparent diffusion coefficient mapping of salivary gland tumors: prediction of the benignancy and malignancy. AJNR Am J Neuroradiol 28:116–121
10. Mukai H, Motoori K, Horikoshi T et al (2016) Basal cell adenoma of the parotid gland; MR features and differentiation from pleomorphic adenoma. Dentomaxillofac Radiol 45:20150322
11. Yuan Y, Tang W, Tao X (2016) Parotid gland lesions: separate and combined diagnostic value of conventional MRI, diffusion-weighted imaging and dynamic contrast-enhanced MRI. Br J Radiol 89:20150912
12. Xu XQ, Hu H, Su GY et al (2016) Utility of histogram analysis of ADC maps for differentiating orbital tumors. Diagn Interv Radiol 22:161–167
13. Suo ST, Zhang KB, Cao MQ et al (2016) Characterization of breast masses as benign or malignant at 3.0T MRI with whole-lesion histogram analysis of the apparent diffusion coefficient. J Magn Reson Imaging 43:894–902
14. Zhang YD, Wu CJ, Wang Q et al (2015) Comparison of utility of histogram apparent diffusion coefficient and R2* for differentiation of low-grade from high-grade clear cell renal cell carcinoma. AJR Am J roentgenol 205:W193–W201
15. Xu XQ, Ma G, Wang YJ et al (2017) Histogram analysis of diffusion kurtosis imaging of nasopharyngeal carcinoma: correlation between quantitative parameters and clinical stage. Oncotarget 8:47230–47238
16. Liang HY, Huang YQ, Yang ZX, Ying D, Zeng MS, Rao SX (2015) Potential of MR histogram analyses for prediction of response to chemotherapy in patients with colorectal hepatic metastases. Eur J radiol 26:2009–2018
17. DeLong ER, DeLong DM, Clarke-Pearson DL (1988) Comparing the areas under two or more correlated receiver operating characteristic curves: a nonparametric approach. Biometrics 44:837–845
18. Fruehwald-Pallamar J, Czerny C, Holzer-Fruehwald L et al (2013) Texture-based and diffusion-weighted discrimination of parotid gland lesions on MR images at 3.0 T. NMR Biomed 26:1372–1379
19. Sumi M, Van CM, Sumi T, Obara M, Ichikawa Y, Nakamura T (2012) Salivary gland tumors: use of intravoxel incoherent motion MR imaging for assessment of diffusion and perfusion for the differentiation of benign from malignant tumors. Radiology 263:770–777
20. Ikeda M, Motoori K, Hanazawa T et al (2004) Warthin tumor of the parotid gland: diagnostic value of MR imaging with histopathologic correlation. AJNR Am J Neuroradiol 25:1256–1262
21. Tao X, Yang G, Wang P et al (2017) The value of combining conventional, diffusion-weighted and dynamic contrast-enhanced MR imaging for the diagnosis of parotid gland tumours. Dentomaxillofac Radiol 46:20160434
22. Xu XQ, Hu H, Su GY, Liu H, Shi HB, Wu FY (2016) Diffusion weighted imaging for differentiating benign from malignant orbital tumors: diagnostic performance of the apparent diffusion coefficient based on region of interest selection method. Korean J Radiol 17:650–656